XIII. PLASMA MAGNETOHYDRODYNAMICS AND ENERGY CONVERSION*

Prof. G. A. Brown
Prof. E. N. Carabateas
Prof. S. I. Freedman
Prof. W. H. Heiser
Prof. M. A. Hoffman
Prof. W. D. Jackson
Prof. J. L. Kerrebrock
Prof. H. P. Meissner
Prof. J. R. Melcher
Prof. G. C. Oates
Prof. J. P. Penhune
Prof. J. M. Reynolds III
Prof. A. H. Shapiro
Prof. J. L. Smith, Jr.
Prof. R. E. Stickney
Prof. H. H. Woodson
Dr. R. Toschi
A. A. Aponick
E. R. Babcock
M. T. Badrawi
J. F. Carson
A. N. Chandra
R. S. Cooper
J. M. Crowley
R. Dethlefsen
M. G. A. Drouet
D. A. East
J. R. Ellis, Jr.
M. R. Epstein
F. W. Fraim IV
J. W. Gadzuk
J. Gerstmann
N. Gothard
J. B. Heywood
R. M. Jansen
H. D. Jordan
P. G. Katona
F. D. Ketterer
G. B. Kliman
A. G. F. Kniazzeh
H. C. Koons
M. F. Koskinen
K. S. Lee
R. F. Lercari
W. H. Levison
A. T. Lewis
H. C. McClees, Jr.
C. W. Marble
T. D. Masek
J. T. Musselwhite
S. A. Okereke
J. H. Olsen
C. R. Phipps, Jr.
E. S. Pierson
D. H. Pruslin
M. H. Reid
C. W. Rook, Jr.
A. W. Rowe
M. R. Sarraquigne
A. Shavit
M. N. Shroff
A. Solbes
P. M. Spira
J. S. Weingrad
G. L. Wilson
J. C. Wissmiller
B. M. Zuckerman

A. WORK COMPLETED

1. A-C PROPERTIES OF SUPERCONDUCTORS

The present phase of this work has been completed by C. R. Phipps and the results have been presented in a thesis entitled "Alternating-Current Properties of Superconducting Wires" to the Department of Electrical Engineering, M.I.T., in partial fulfillment of the requirements for the degree of Master of Science, June 1963.

W. D. Jackson

2. HYDROMAGNETIC WAVEGUIDES

The present phase of this work has been completed by M. R. Epstein and the results have been presented in a thesis entitled "Alfvén Wave Propagation in Liquid NaK" to the Department of Electrical Engineering, M.I.T., in partial fulfillment of the requirements for the degree of Bachelor of Science, June 1963.

W. D. Jackson

*This work was supported in part by the National Science Foundation under Grant G-24073, and in part by the U.S. Air Force (Aeronautical Systems Division) under Contract AF33(616)-7624 with the Aeronautical Accessories Laboratory, Wright-Patterson Air Force Base, Ohio.

3. MAGNETOHYDRODYNAMIC VORTEX GENERATOR

This research has been completed by H. D. Jordan and the results have been submitted as an S. B. thesis entitled "An Evaluation of the Vortex-Type Magnetohydrodynamic Generator" to the Department of Electrical Engineering, M. I. T., June 1963.

W. D. Jackson

4. IONIC PLASMA OSCILLATIONS

The present phase of this work has been completed by H. C. Koons and the results have been submitted as an S. B. thesis entitled "Ultrasonic Excitation of Ionic Plasma Oscillations" to the Department of Physics, M. I. T., June 1963.

R. S. Cooper

5. FLOWMETERS FOR BLOOD-FLOW MEASUREMENT[†]

The present phase of this work has been completed and the results have been presented as theses to the Department of Electrical Engineering, M. I. T.

C. W. Marble, "A Thermistor Equipped Thermal Conduction Flowmeter," S. B. Thesis. June 1963.

J. T. Musslewhite, "Design of an Electromagnetic Flowmeter," S. B. Thesis, June 1963.

M. N. Shroff, "Calibration of Electromagnetic Flowmeter for Blood Flow Measurement," S. B. Thesis, June 1963.

W. D. Jackson

6. BLOOD-FLOW STUDIES[†]

The present phase of this work has been completed by M. R. Sarraquigne and the results have been presented in a thesis entitled "A Pressure Function Generator for Blood Flow Studies" to the Department of Electrical Engineering, M. I. T., in partial fulfillment of the requirements for the degree of Bachelor of Science, June 1963.

W. D. Jackson

B. A-C PROPERTIES OF SUPERCONDUCTORS

Investigation of the properties of superconducting coils under alternating current excitation is being pursued to determine the feasibility of using available superconductors

---

[†]This work was supported in part by the National Institutes of Health (Grant HTS-5550).

to fabricate very low loss ac magnetic fields. Both hard and soft superconductors are being tested from dc up to a frequency of 10 kc.

Two quantities characterizing the ac properties of these materials have been measured.

(a) $I_q(\omega)$ the maximum instantaneous supercurrent that can be applied instantaneously.

(b) $I_c(\omega)$ the maximum supercurrent that can be maintained indefinitely without the occurrence of a quench.

The frequency dependence of these two quantities has been found to differ in hard and soft superconductors. Results of tests on solenoids wound with Nb-Zr and lead wires are given in Fig. XIII-1. The procedure for establishing values of I_q was to

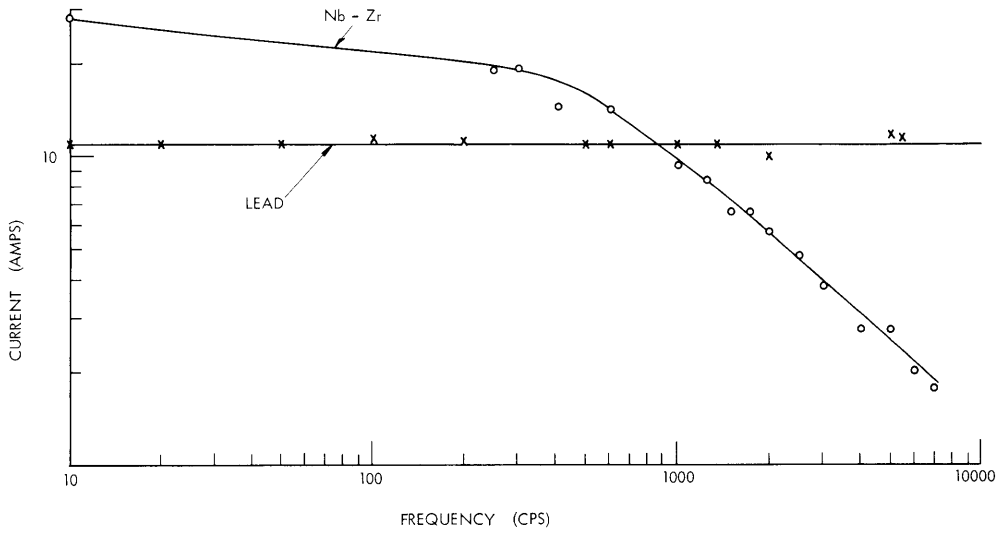

Fig. XIII-1. $I_q(\omega)$ for Nb-Zr and for lead.

increase the solenoid current in approximately 1 second to a value that would cause a rapid quench. By repeated trials, the I_q to obtain a quench in less than 0.5 sec was determined.

Figure XIII-1 shows $I_q(\omega)$ to be independent of frequency in lead, the soft superconductor tested, up to 10 kc, while for Nb-Zr, a hard superconductor, the drop-off in $I_q(\omega)$ with increasing frequency is such that at 7 kc, $I_q(\omega)$ is approximately 7 per cent of the 10-cps value. Hard superconductors are assumed to carry current in internal filaments, whereas soft superconductors carry it in a thin skin at the surface. Changes in $I_q(\omega)$ appear to be controlled by frequency dependence of the filamentary structure, the detailed nature of which is still inknown.

In both hard and soft superconductors, time-delayed quenches could be attained; thus a difference between I_c and I_q is indicated. As illustrated in Figs. XIII-2 and XIII-3,

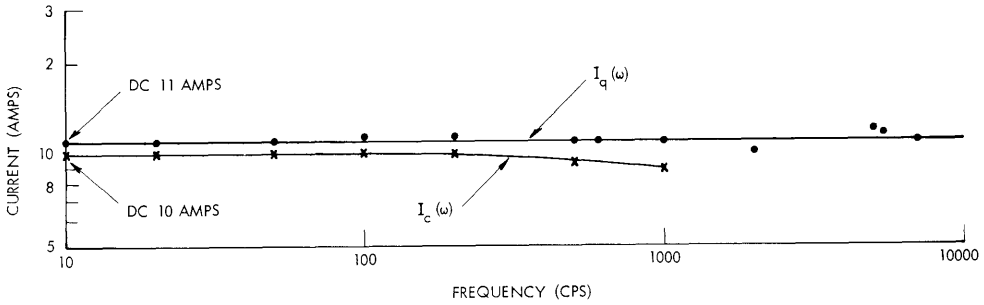

Fig. XIII-2. $I_c(\omega)$ and $I_q(\omega)$ for lead.

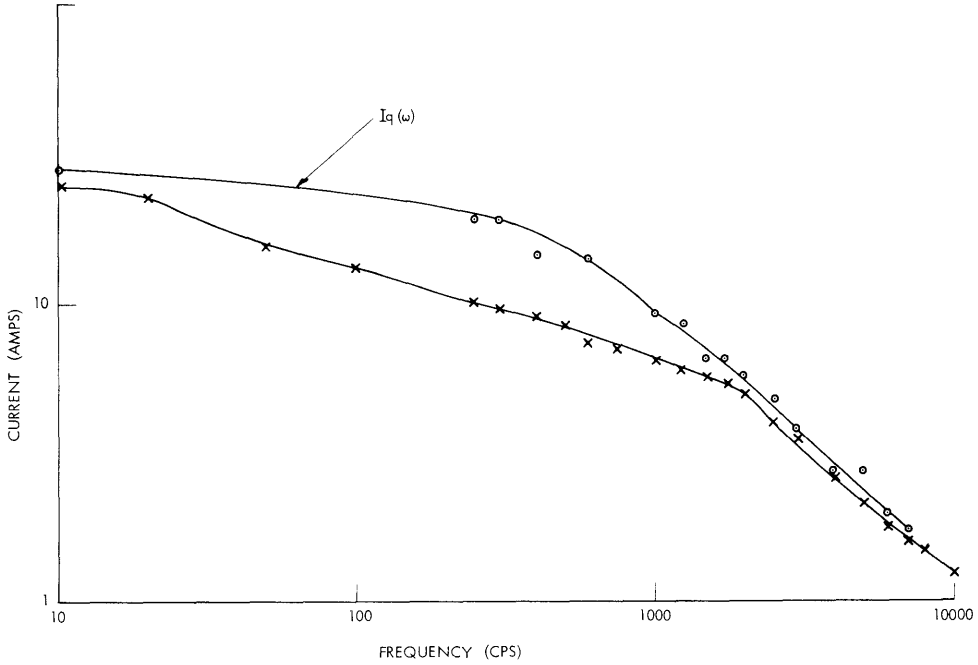

Fig. XIII-3. $I_q(\omega)$ and $I_c(\omega)$ for Nb-Zr.

these occurred in Nb-Zr at much lower frequencies than in lead. These quenches are apparently due to ac loss which heats the specimen to a temperature higher than its critical temperature. They should be more pronounced in hard superconductors, which have an internal field in the ohmic region, and this has been confirmed by experimental observation. In soft superconductors such losses occur in the surface region only.

This note is based on two recent theses[1,2] presented to the Department of Electrical Engineering, M. I. T. Further work is contemplated to confirm and extend the results thus far obtained.

W. D. Jackson, C. R. Phipps, Jr., P. M. Spira

References

1. C. R. Phipps, Alternating-Current Properties of Superconducting Wires, S. M. Thesis, Department of Electrical Engineering, M. I. T., June 1963.

2. P. M. Spira, Superconducting Coil Properties with Alternating Current Excitations, S. B. Thesis, Department of Electrical Engineering, M. I. T., June 1963.

C. LANGMUIR-MODE ANALYSIS OF THE PLASMA THERMIONIC-ENERGY CONVERTER

1. Introduction

Under certain conditions of emitter temperature and cesium pressure the voltage-current characteristic of a cesium thermionic converter exhibits two branches. The upper branch, at higher output power and efficiency, is considered as a Langmuir-mode gaseous electric discharge. The Langmuir-mode discharge[1] is characterized by a neutral plasma joined to the emitter by a double sheath and to the collector with a unipolar sheath.

Ions are created in the interelectrode spacing by inelastic collisions of the electrons. These ions diffuse to the emitter and collector, and thus decrease the potential barrier in front of the emitter and permit a larger electron current to flow.

In the present report an analysis of the Langmuir-mode discharge based on the following model is carried out.

Electrons are emitted from the cathode at A on the motive diagram of Fig. XIII-4, pass over C (the top of the potential barrier), and fall through the thin double sheath CD and the presheath DE, and finally enter the cesium plasma at E. On entering the plasma the electron velocities are immediately randomized by collisions with Cs atoms and Maxwellianized by collisions with each other. The electron current spilling over the barrier is limited by the ion current falling from the plasma back to the cathode according to the Langmuir double-sheath condition.[2] Ions are generated in the plasma by a cumulative process, and diffuse to the electrodes by ambipolar diffusion. The total ionization probability is determined to be an eigenvalue to the ion-diffusion equation and the electron temperature is found by satisfying the electron-energy equation. These equations are sufficient to permit calculation of I-V curves (as shown in Fig. XIII-9) for different values of p_o the reduced cesium pressure, d the diode spacing, T_E the emitter temperature, and T_C the collector temperature. These calculations were performed by choosing two constants pertaining to the excitation and ionization rates so that the theoretical and experimental curves[3] would coincide at one data point. The derivation is presented below.

2. Diffusion Equation

Transport in the plasma is by ambipolar diffusion with a charge-transfer cross section.[4]

$$j_p = -D_a \nabla n_e - \frac{\mu_p}{\mu_e} j_e$$

$$\nabla \eta = -\frac{\nabla n_e}{n_e} - \frac{j_e}{n_e D_e} \tag{1}$$

$$\eta \equiv \frac{eV}{kTe} \qquad D_a = \frac{3\pi\sqrt{2}}{8} \lambda_p \frac{\bar{c}_p}{4} \left(\frac{T_e}{T_p} + 1 \right)$$

$$\lambda_p = \frac{1}{9300 p_o} \qquad \bar{c}_p \equiv \sqrt{\frac{8kT_p}{\pi M}}$$

Excited 6p atoms are generated by electron-atom collisions at a rate

$$\frac{dn^*}{dt} = a_1 n_e$$

where

$$a_1 = \alpha_1 p_o F_1$$

$$F_1 = 1.97 \times 10^7 \left(\frac{T_e}{10^3} \right)^{1/2} \left(1.39 + \frac{T_e}{5800} \right) \exp\left(- \frac{16.15 \times 10^3}{T_e} \right).$$

Ions are generated by electron-atom collisions at a rate

$$\frac{dn_e}{dt} = a_2 \frac{n^*}{n_a} n_e$$

where

$$a_2 = \alpha_2 p_o F_2$$

$$F_2 = 1.97 \times 10^7 \left(\frac{T_e}{10^3} \right)^{1/2} \left(2.5 + \frac{T_e}{5800} \right) \exp\left(- \frac{29 \times 10^3}{T_e} \right).$$

Excited atoms are lost by imprisoned resonance radiation having an effective lifetime $\tau = 2.55 \times 10^{-6}$ sec. In a steady state

$$a_1 n_e = \frac{n^*}{\tau}.$$

Ions are lost by diffusion

$$-D_a \nabla^2 n_e = \nabla \cdot j_p = a_2 \frac{n^*}{n_a} n_e = a_1 a_2 \tau \frac{n_e^2}{n_a}.$$

In one dimension,

$$\frac{d^2 z}{d\xi^2} = -\frac{3}{2} z^2$$

$$z \equiv \frac{n_e}{n_{eo}} \qquad \xi \equiv \frac{x}{\ell} \tag{2}$$

$$\ell^2 \equiv \frac{3}{2} \frac{D_a}{a_1 a_2 \tau \frac{n_{eo}}{n_a}}.$$

The diffusion equation is solved by using the transformation

$$z = \cos^{2/3} \theta \qquad \frac{dz}{d\xi} = -\sin \theta$$

$$\frac{d\theta}{d\xi} = \frac{3}{2} \cos^{1/3} \theta \qquad \xi \approx 1.403 - \cos^{2/3} \theta.$$

At the plasma boundary the ion current equals the random-ion current.

$$j_p = n_e \frac{\bar{c}_p}{4}.$$

At the emitter edge,

$$\cos^{2/3} \theta_E = \frac{4.66 \frac{\lambda_p}{d} \left(\frac{T_e}{T_p} + 1 \right)}{\left[1 + 3.32 \frac{\lambda_p}{d} \left(\frac{T_e}{T_p} + 1 \right) \right] (1-R)}.$$

At the collector edge,

$$\cos^{2/3} \theta_C = (1-2R) \cos^{2/3} \theta_E$$

where

$$R \equiv \frac{\mu_p}{\mu_e} \frac{j_e}{j_{pE}}.$$

The mobilities for ions and electrons are evaluated[5,6] to be

$$\mu_p = \frac{e}{kT_p} \frac{3\pi\sqrt{2}}{8} \lambda_p \frac{\bar{c}_p}{4} \qquad \mu_e = \frac{e}{kT_p} \frac{1}{3} \lambda_e \bar{c}_e.$$

$$\frac{\lambda_p}{\lambda_e} = \frac{P_{C(e)}}{P_{C(p)}} = \frac{1200}{9300}.$$

Therefore

$$R = 0.161 \left(\frac{T_e}{T_p}\right)^{1/2} G$$

where

$$G \equiv \left(\frac{m}{M}\right)^{1/2} \frac{j_e}{j_{pE}}.$$

It will be shown that $G \leq 1$, so that R is always small.

The ion currents to the emitter and collector are

$$j_{pE} = \frac{n_{eo}}{\ell} D_a (1-R)^{-1}$$

$$j_{pC} = (1-2R)\, j_{pE}.$$

The potential drop in the plasma (EF in Fig. XIII-4) is determined by integrating Eq. 1 for the reduced field. For small R the result is

$$\eta_e - \eta_a \approx \frac{G}{1-R} \left[1.54 - 0.14 \frac{T_e}{10^3} + \left(0.5\ 4 + 0.050 \frac{T_e}{10^3}\right) \ln\left(\frac{P_C p_o d}{100}\right)\right]. \qquad (3)$$

3. Electron-Energy Equation

Electrons enter the plasma with an average kinetic energy corresponding to their original heat of transport plus the energy gained in dropping down the cathode fall (CE in Fig. XIII-4). They leave the plasma with a different energy, corresponding to the energy necessary to traverse the barrier GH plus the heat of transport. While in the plasma, the electrons lose energy by exciting and ionizing atoms. In the steady state the net energy carried into the plasma by electrons must equal the energy carried out by radiation and ion transport. These various terms are

Radiation: $\int e(1.39)\frac{n^*}{\tau}\,dx = \int e(1.39)\,a_1 n_e\,dx = 0.305\,\frac{a_1 d^2}{D_a}\,ej_{pE}(1-R)$.

Ion transport: $e(3.89)(j_{pE}+j_{pC}) = 7.78ej_{pE}(1-R)$.

Net electron transport in: $ej_e\left[\Delta V - \frac{2k}{e}(T_e-T_E)\right] - ej_b\,\frac{2k}{e}(T_e-T_E)$

$$- ej_{pE}(1-R)\,2\left(\frac{2kT_e}{e} + V_a\right).$$

The first term in the net electron transport is due to the net electron current j_e; ΔV is the effective plasma drop CH. The second term is due to transport of energy to the cathode which, in turn, is due to the current emitted back from the plasma j_b; the third

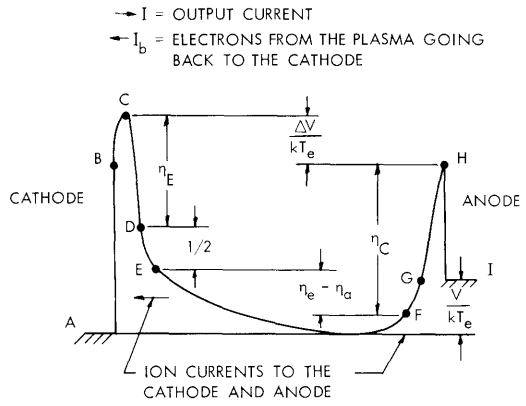

A	CATHODE FERMI LEVEL
I	ANODE FERMI LEVEL
AI	OUTPUT VOLTAGE, $\frac{V}{kT_e}$
CH	EFFECTIVE PLASMA DROP
AB	CATHODE WORK FUNCTION
AC	EFFECTIVE CATHODE WORK FUNCTION
CD	LANGMUIR DOUBLE SHEATH POTENTIAL
DE	CATHODE PRESHEATH
EF	PLASMA DROP
FG	ANODE PRESHEATH
GH	ANODE SHEATH
FH	EFFECTIVE ANODE SHEATH
HI	ANODE WORK FUNCTION

Fig. XIII-4. Motive diagram for the Langmuir mode.

term accounts for the fact that the electron current at the anode differs from that at the cathode by the net ion production in the plasma. It is assumed that an electron makes its last collision at the edge of the plasma (F in Fig. XIII-4) on its way to the anode; V_a is the effective anode sheath height (HF in Fig. XIII-4).

Equating the energy sources and losses for the plasma electrons gives

$$\eta_1 \frac{G}{1-R} = 3.98 \times 10^{-7}\, a_1 P_C (p_o d)^2 \frac{F_1}{\frac{T_e}{10^3}\left(\frac{T_e}{T_p}+1\right)}, \tag{4}$$

where

$$\eta_1 \equiv \frac{\Delta V}{kT_e} - 2\left(1-\frac{T_E}{T_e}\right) - 2\left(\frac{m}{M}\right)^{1/2}\left(\frac{3.89\times 11,605}{T_e}+\frac{V_a}{kT_e}+2\right)\frac{(1-R)}{G} - 2\left(1-\frac{T_E}{T_e}\right)\frac{j_b}{j_e}. \tag{5}$$

The relation between G and η_1 (defined below) provides the last equation required for the calculation of the voltage-current curves for the diode.

4. Langmuir Double-Sheath Condition

The last important relation is derived by integrating Poisson's equation across the cathode double sheath. With the conditions that the electric field is zero at the potential maximum and at the plasma edge of the sheath (C and D of Fig. XIII-4), and that the charge density is zero at D, one finds a relation[2] between the sheath voltage and the ratio of the electron and ion currents passing through the sheath.

$$G = G\left(\eta_E, \frac{T_E}{T_e}, \frac{T_{p\ eff}}{T_e}\right), \tag{6}$$

where η_E is the reduced voltage corresponding to CD in Fig. XIII-4.

The Bohm criterion[7] for the formation of a nonoscillatory sheath fixes a limit on $T_{p\ eff}$, the effective temperature of the ions leaving the presheath: $T_{p\ eff}/T_e \geq 0.5$. G is plotted as a function of η_E for various T_E/T_e and for $T_{p\ eff}/T_e = 0.5$ in Fig. XIII-5. G approaches 1 as η_E becomes very large but is usually approximately 0.5.

The Bohm criterion also predicts the presheath voltage (DE in Fig. XIII-4) to be $0.5kT_e$.

The Langmuir condition also relates the back current and the forward current across the sheath:

$$\frac{j_b}{j_e} = \left[\frac{\sqrt{2}}{G} - \frac{1}{\sqrt{\eta_E + \frac{T_E}{T_e}}}\right]\left[2\sqrt{\pi}\,\exp\eta_E + \frac{1}{\sqrt{\eta_E+\frac{T_E}{T_e}}} - \frac{1}{\sqrt{\eta_E+1}}\right]^{-1}. \tag{7}$$

The height of the unipolar anode sheath is given by the Boltzmann factor

$$\exp\eta_C(1+\mathrm{erf}\sqrt{C}) = 2\left(\frac{T_e}{T_p}\right)^{1/2}\frac{(1-R)}{G}. \tag{8}$$

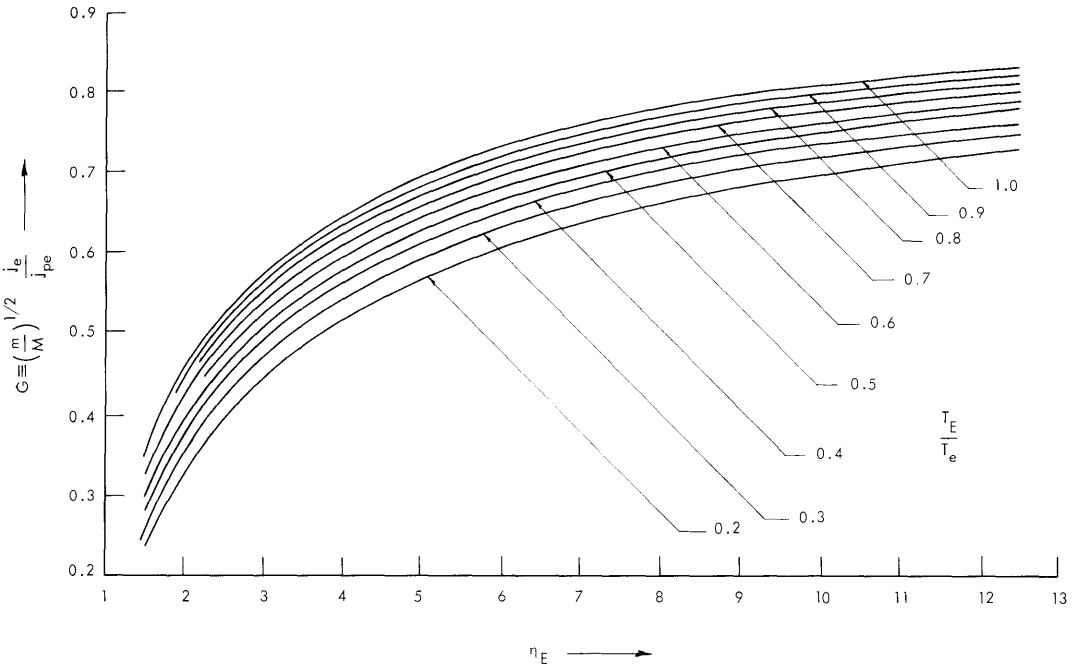

Fig. XIII-5. Langmuir double-sheath condition $T_{p\ eff} = 0.5T_e$.

Equations 3 and 5-8 are combined to give $\frac{G}{1-R}$ as a function of

$$\eta_2 \equiv \eta_1 - \frac{G}{(1-R)}\left(0.564 + 0.050\,\frac{T_e}{10^3}\right)\ln\left(\frac{P_C p_o d}{100}\right),$$

as shown in Fig. XIII-6. These curves are approximated by straight lines to give

$$\frac{G}{1-R} = \frac{0.255 + 0.041\,\frac{T_e}{10^3} + 0.103\eta_1}{1 + \left(0.057 + 0.005\,\frac{T_e}{10^3}\right)\ln\left(\frac{P_C p_o d}{100}\right)} \qquad \text{if } \frac{G}{1-R} < 0.57 \tag{9}$$

$$\frac{G}{1-R} = \frac{0.387 + 0.02\,\frac{T_e}{10^3} + 0.065\eta_1}{1 + \left(0.037 + 0.0032\,\frac{T_e}{10^3}\right)\ln\left(\frac{P_C p_o d}{100}\right)} \qquad \text{if } \frac{G}{1-R} > 0.57$$

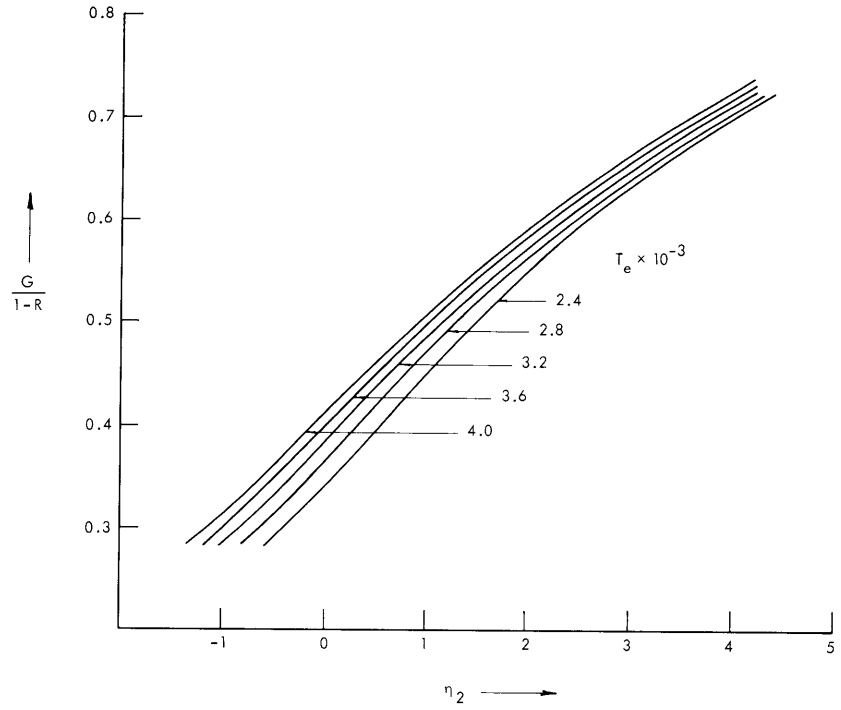

Fig. XIII-6. $\frac{G}{1-R}(\eta_2)$ for $T_E = 1600°K$, $T_e = 1200°K$.

5. Voltage-Current Relation

Equations 4 and 9 are combined to give a noniterative procedure for generating the voltage-current curves. The energy equation is

$$\eta_1 g = 0.0397 a_1 P_C (p_o d)^2 f \frac{F_1}{10^2 T_e \left(\frac{T_e}{T_p} + 1\right)}, \tag{10}$$

where

$$g \equiv 0.255 + 0.041 T_e/10^3 + 0.103\eta_1$$

$$f \equiv 1 + 0.072 \ln\left(\frac{P_C p_o d}{100}\right).$$

Evaluating ℓ from the boundary conditions and using Eq. 2 gives

$$\eta_1 I = \frac{0.122}{a_2 \tau P_C p_o d} \frac{10^8 \left(\frac{T_e}{T_p} + 1\right)}{F_2 T_e}. \tag{11}$$

Here, the temperature function is approximated by

$$\frac{F_2 T_e}{10^8\left(\frac{T_e}{T_p}+1\right)} = 1.3\left[\frac{F_1}{10^2 T_e\left(\frac{T_e}{T_p}+1\right)}\right]^{2.32} . \tag{12}$$

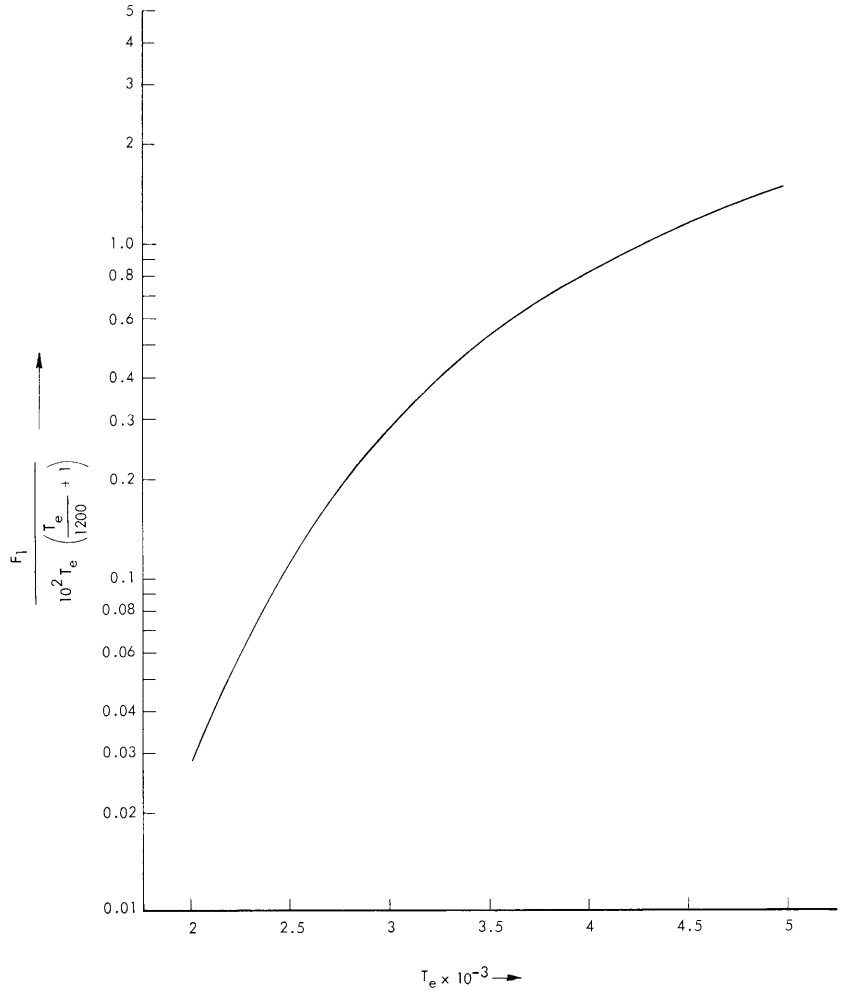

Fig. XIII-7. $\frac{F_1}{10^2 T_e\left(\frac{T_e}{1200}+1\right)}$ versus T_e.

Equations 10-12 give

$$\eta_1 = AC^{-.7} \tag{13}$$

$$\frac{F_1}{10^2 T_e\left(\frac{T_e}{T_p}+1\right)} = BC^{+.3} \tag{14}$$

where

$$A \equiv 0.0516 \frac{a_1^{.7}}{(a_2\tau)^{.3}} (p_o d)^{1.1} P_C^{.4} \left[1 + 0.072 \ln\left(\frac{P_C p_o d}{100}\right)\right]^{.3} I^{-.3}$$

$$B \equiv 1.3 \left[I a_1 a_2 \tau \left\{1 + 0.072 \ln\left(\frac{P_C p_o d}{100}\right)\right\}\right]^{-.3} (p_o d)^{-.9} P_C^{-.6}$$

$$C \equiv 0.353 + 0.069B + 0.169A.$$

In Fig. XIII-7, $F_1/10^2 T_e\left(\frac{T_e}{T_p} + 1\right)$ is plotted for $T_p = 1200°K$. The back current and ion loss term is plotted in Fig. XIII-8. For a given value of I, the output current in amp/cm^2, η_1, and T_e are found from Eqs. 13 and 14 and Fig. XIII-7. G/(1-R) is found

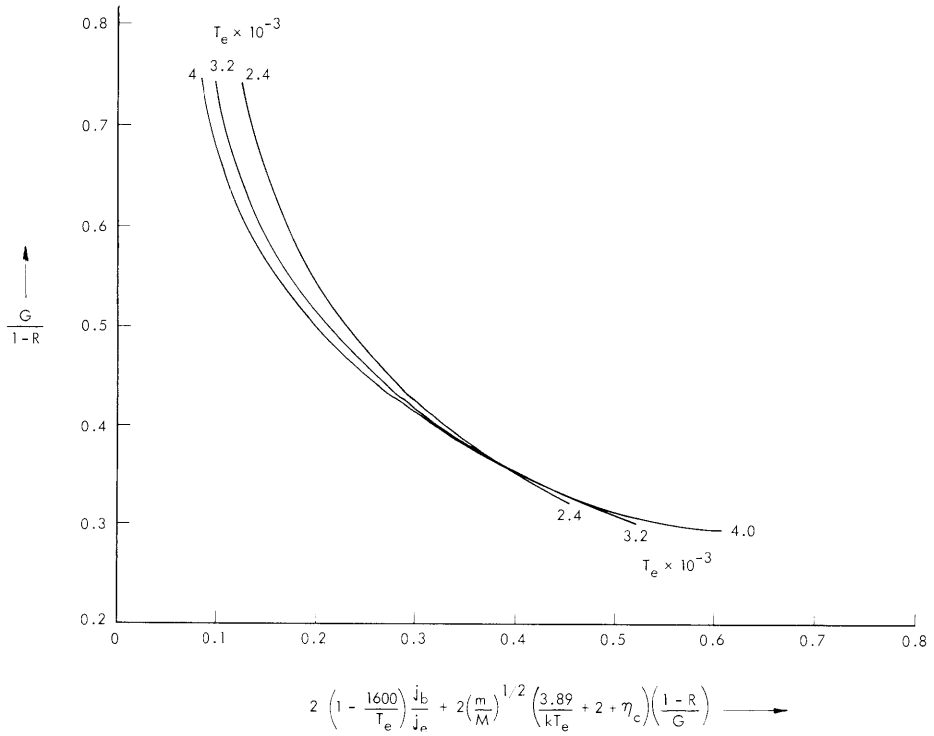

Fig. XIII-8. Back emission and ionization losses. $T_E = 1600°K$, $T_p = 1200°K$.

from Fig. XIII-8. This is added to η_1, along with $2\left(1 - \frac{T_E}{T_e}\right)$, to give $\frac{\Delta V}{kT_e}$ and then ΔV. Now that I and ΔV are known, the output voltage V can be found if ϕ_C, the collector

work function, is known:

$$V = \phi_m - \phi_C - V,$$

where ϕ_m is found from I and T_E by Richardson's equation.[8] Thus for given values of the diode parameters d, p_o, T_E, and ϕ_C the voltage-current curve can be found.

Theoretical I-V curves were calculated in this way and are plotted in Fig. XIII-9, along with experimental curves for the same conditions. Since accurate values of the excitation and ionization coefficients a_1 and a_2 are not available, the calculation was made by using the a_1 and a_2 that fit experimental data at one data point (shown in Fig. XIII-9) at an assumed electron temperature of 3000°K and a collector work function of 1.6 volts. This procedure results in $a_1 = 4.77$ and $a_2 = 691$.

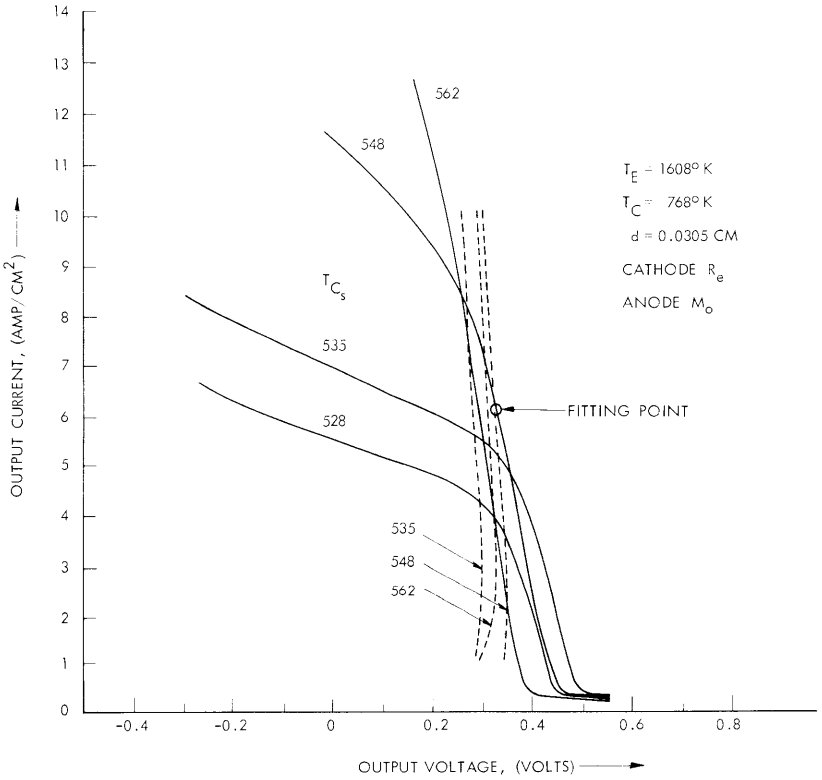

Fig. XIII-9. I-V curves from experiment (solid curves) and from theory (dashed curves, for the Langmuir-mode model).

Although these a's disagree by a factor of 7 with other estimates, the voltage-current curves derived from the model bear close resemblance to the experimental curves. The experimental curves bend over at high currents when the diode draws saturation current

from part of the emitter surface; this effect was not included in the model. The pressure dependence of the output voltage at constant current is close to that expected, although the reversal should occur at a lower cesium pressure approximately 535°K instead of 548°K. This suggests that the assumed plasma electron temperature at the fitting point is low. The slopes of the theoretical curves are not as great as the experimental ones, although some improvement would be evident if the ion current and the back current were not neglected in calculating ϕ_m from Richardson's equation.

In conclusion, it is felt that a model of the Langmuir-mode discharge can predict the essential features of experimental voltage-current curves of a thermionic diode. Several improvements of the model are suggested by this analysis: consideration of de-excitation by electron-excited atom collisions, recombination, alternative ionization mechanisms, and energy exchange by elastic recoil.

A. G. F. Kniazzeh, E. N. Carabateas

References

1. E. O. Johnson, RCA Review 16, 498 (1955).

2. I. Langmuir, Phys. Rev. 33, 954 (1929).

3. Thermo-Electron Engineering Corporation unpublished plasma thermionic diode data, Rhenium tube #2, Run 14 (1963).

4. J. W. Sheldon, J. Appl. Phys. 34, 444 (1963).

5. S. Chapman and T. G. Cowling, Mathematical Theory of Non-Uniform Gases (Cambridge University Press, London, 1960).

6. S. C. Brown, Basic Data of Plasma Physics (The Technology Press of Massachusetts Institute of Technology, Cambridge, Mass., and John Wiley and Sons, Inc., New York, 1959).

7. D. Bohm, Characteristics of Electrical Discharges in Magnetic Fields, edited by A. Guthrie and R. K. Wakerling (McGraw-Hill Book Company, Inc., New York, 1949), Chapter 3.

8. W. T. Norris, Thermionic Emission From a Single Crystal of Tantalum Exposed to Cesium Vapor, Sc.D. Thesis, Department of Mechanical Engineering, M.I.T. August 1962.

D. CALCULATION OF MONOPOLE WORK

It has been shown previously[1] that the work function ϕ of a conductor can be written

$$\phi = M + D - \zeta, \tag{1}$$

where D (called dipole work) is the electronic charge times the difference in electrostatic potential between the inside and the outside of the conductor, ζ is the electron degeneracy energy, and M is defined by Eq. 1. It was suggested that M could be identified with a sort of "image-force work" called monopole work. This report shows a

simple method of estimating the monopole work.

When the distance x of an electron from the plane of effective charge is great, the monopole force is given by the ideal image force F(x). Therefore, the monopole work will be written

$$M = -\int_0^\infty g(x)\, F(x)\, dx,$$

where g(x) is determined by the nature of the material in question. When x is larger than a few atomic radii, g(x) equals unity. When x approaches zero, g(x) approaches zero.

The difference in monopole work ΔM_{12} between two geometrically different conductors is

$$\Delta M_{12} = \int_0^\infty g(x)\, F_1(x)\, dx - \int_0^\infty g(x)\, F_2(x)\, dx,$$

where $F_1(x)$ and $F_2(x)$ are the associated image forces computed on the basis of ideal conductors. Note that for small x, $F_1(x)$ approximately equals $F_2(x)$, that is, F(x) for a semi-infinite solid. ΔM_{12} can also be written

$$\Delta M_{12} = \int_0^\delta g(x)\, [F_1(x) - F_2(x)]\, dx + \int_\delta^\infty g(x)\, [F_1(x) - F_2(x)]\, dx,$$

where δ is a constant. If δ is selected to be small enough, the first integral is very nearly zero and can be replaced by

$$\int_0^\delta [F_1(x) - F_2(x)]\, dx,$$

which is also very nearly zero. If, at the same time, δ can be taken to be large enough so that $g(\delta)$ is very nearly unity, then g(x) can be eliminated from the second integral, and ΔM_{12} is written

$$\Delta M_{12} = \int_0^\infty [F_1(x) - F_2(x)]\, dx \tag{2}$$

subject to the two conditions; there exists a distance δ such that

$$g(\delta) \approx 1 \tag{3}$$

and

$$F_1(\delta) \approx F_2(\delta). \tag{4}$$

To meet the first condition, δ should be greater than a few atomic diameters. The

second condition is met when δ is small in comparison with the curvature of the surface.

Consider the difference in monopole work between a semi-infinite solid and an ungrounded sphere of radius a. By the method of images,

$$F_1(x) = -\frac{e^2}{4\pi\epsilon_o}\frac{1}{4x}$$

$$F_2(x) = -\frac{e^2}{4\pi\epsilon_o}\left[\frac{a/r}{(r-a^2/r)^2} + \frac{1-a/r}{r^2}\right],$$

where e is the electronic charge and r = a + x. To evaluate the integral of Eq. 2, integrate $F_1(x)$ and $F_2(x)$ separately from $x = \eta$ to $x = \infty$, take the difference, and then let η go to zero, being careful not to drop the $(-1/8a)$ term from the first part of $F_2(x)$. The result is

$$\Delta M_{12} = \frac{e^2}{4\pi\epsilon_o}\frac{3}{8a} = 5.4/a, \tag{5}$$

where ΔM_{12} is in electron volts and a is in angstroms. That is, the monopole work of a small ungrounded sphere is slightly greater than that of a semi-infinite solid (0.01 ev for a 1000 Å sphere).

By Eq. 1, if one assumes that D and ζ are not functions of crystal size, the work function (more precisely, the first ionization potential) V_a of a small sphere of radius a is given by

$$V_a = \phi_o + 3e^2/16\pi\epsilon_o a, \tag{6}$$

where ϕ_o is the work function of a semi-infinite solid.

Rowe and Kerrebrock (Section XIII-F) have applied this formula to the ionization potential of alkali-metal droplets in order to compute the electrical conductivity of the vapor. In Rowe's case, for at least 100 atoms per droplet, conditions (3) and (4) are reasonably well met. Quantum-mechanical calculations by Bardeen[2] based on a model which takes the structure of the metal into account indicate that the force on an electron outside the surface of a metal is just the classical image force. By applying Eq. 6 to a single atom, Table XIII-1 shows the computed work function ϕ_o of a semi-infinite solid, obtained from the first ionization potential[3] V_a of the free atom and the atomic radius a.[3] The measured work function[4] ϕ is given, as is the discrepancy $\phi - \phi_o$. The explanation of this discrepancy is still not complete, but a partial explanation can be given.

For the alkali metals (I): Since the kinetic energy of the valence electron is approximately equal to the electron-degeneracy of the solid, the assumption that $\Delta\zeta = 0$ seems reasonable. Having only one valence electron, the free atom has zero "surface double layer." Therefore, $\phi - \phi_o$ should equal the dipole work D of the solid metal, which is

Table XIII-1. Work function ϕ_o of the elements, computed from Eq. 6, compared with the reported values of the work function ϕ.

	V_a [a] (ev)	a [a] (Å)	ΔM_{12} [b] (ev)	ϕ_o [c] (ev)	ϕ [d] (ev)	$\phi - \phi_o$ (ev)
I						
Lithium	5.40	1.55	3.48	1.92	2.49	0.57
Sodium	5.14	1.90	2.84	2.30	2.28	-0.02
Potassium	4.34	2.35	2.30	2.04	2.24	0.20
Rubidium	4.17	2.48	2.18	1.99	2.09	0.10
Cesium	3.89	2.67	2.02	1.87	1.81	-0.06
II						
Beryllium	9.32	1.12	4.82	4.50	3.92	-0.58
Magnesium	7.64	1.60	3.37	4.27	3.68	-0.59
Calcium	6.11	1.97	2.74	3.37	2.71	-0.66
Strontium	5.69	2.15	2.51	3.18	2.74	-0.44
Barium	5.21	2.22	2.43	2.78	2.48	-0.30
III						
Titanium	6.84	1.47	3.67	3.17	3.95	0.78
Zirconium	6.95	1.60	3.37	3.58	4.21	0.63
Niobium	6.77	1.46	3.70	3.07	4.01	0.94
Molybdenum	7.06	1.39	3.89	3.17	4.20	1.03
Tungsten	7.94	1.39	3.89	4.05	4.52	0.47
Rhenium	7.87	1.37	3.94	3.93	5.10	1.17
Cobalt	7.84	1.25	4.32	3.52	4.40	0.88
Rhodium	7.7	1.34	4.03	3.70	4.80	1.10
Palladium	8.1	1.37	3.94	4.16	4.98	0.82
Platinum	8.96	1.39	3.89	5.07	5.34	0.27
Copper	7.72	1.28	4.22	3.50	4.46	0.96
Silver	7.58	1.44	3.75	3.83	4.73	0.90
IV						
Aluminum	5.97	1.43	3.78	2.19	4.08	1.89
Carbon	11.27	0.91	5.93	5.34	4.60	-0.74
Nickel	7.63	1.24	4.36	3.27	5.01	1.74
Gold	9.23	1.44	3.75	5.48	4.82	-0.66
Cadmium	8.99	1.54	3.51	5.48	4.07	-1.41
Mercury	10.44	1.57	3.44	7.00	4.53	-2.47
Bismuth	8.8	1.70	3.18	5.62	4.24	-1.38

a. See Periodic Chart of the Elements.[3]

b. Eq. 5.

c. Eq. 6.

d. See Handbook of Chemistry and Physics.[4]

a little less than 0.5 ev for the alkali metals.[5]

For the alkaline earths (II): The assumption that $\Delta\zeta = 0$ is probably not quite as good, but is still reasonable. The free atom has a moderately strong positive "surface double layer" that can be identified with the shielding coefficient of the valence electron left on the atom after the atom has been singly ionized. $\phi - \phi_o$ should be small or slightly negative.

Because of their complexity, no further comment is offered for the remaining elements, except to note that $\phi - \phi_o$ for elements from the center of the periodic table (part III of Table XIII-1) is of the order of magnitude of the surface double layer, 0.25-1 electron volt.[1,5,6]

This method of predicting monopole work will be explored further.

M. F. Koskinen

References

1. M. F. Koskinen, Work function of a conductor, Quarterly Progress Report No. 68, Research Laboratory of Electronics, M.I.T., January 15, 1963, pp. 108-113.

2. J. Bardeen, Phys. Rev. 58, 727 (1940).

3. Periodic Chart of the Elements, RCA Laboratories, Princeton, N.J. (1955).

4. Handbook of Chemistry and Physics (Chemical Rubber Publishing Company, Cleveland, 40th edition, 1958-1959).

5. J. Bardeen, Phys. Rev. 49, 655 (1936).

6. E. Wigner and J. Bardeen, Phys. Rev. 48, 85 (1935).

E. EMITTER WORK-FUNCTION PATCHES IN A CESIUM THERMIONIC CONVERTER

1. Introduction

An experimental program to obtain current-voltage characteristics from a metal cesium thermionic converter with a single-crystal (110) molybdenum emitter has been carried out. The results of this program are presented in this report. The output characteristics obtained experimentally are of the type that would be expected if a fraction of the emitter surface had a low work-function patch, the distribution of work function on this patch being given by an exponential Boltzmann type of distribution. The remainder of the surface has a discrete work function. The results of our analysis apply in the presence of transport effects in the interelectrode space. We find that the percentage of the area of the exponential patch increases as the cesium coverage increases.

2. Apparatus

A metal cesium thermionic converter has been designed and constructed specifically for the purpose of conducting laboratory tests. The diode configuration is of a parallel-plate nature with circular electrodes, 1 cm^2 in area, spaced 0.01 inch apart. A single-crystal molybdenum emitter was exposed to the cesium vapor. A complete description of the device has been given elsewhere.[1] The experimental apparatus, test circuit, and procedure have been presented in detail.[2] The testing consisted of setting a certain emitter and cesium temperature, and then obtaining the resulting I-V curve.

3. Theory

The purpose of this project was to offer an explanation for current-voltage curves of the form that display a linear increase in output current with decreasing output voltage in the region in which saturation current is expected, region B of Fig. XIII-10a. The theoretical treatment is presented in the author's thesis,[2] and only the major points are given here.

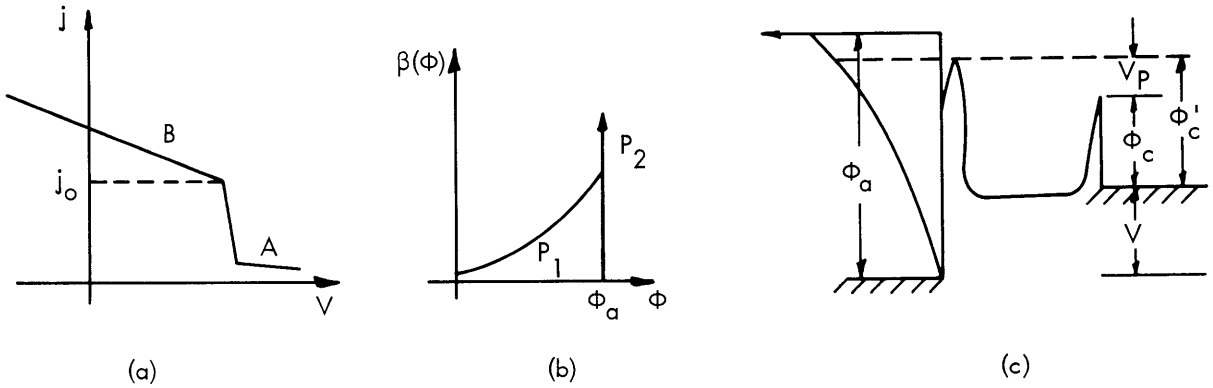

Fig. XIII-10. (a) Typical I-V curve; (b) Distribution of work function; (c) Motive diagram for operation in region B.

From physical considerations it is expected that a surface partially covered with cesium will have a Boltzmann distribution of work function over a fraction of its area. This is given by

$$B(\phi) = \frac{P_1}{kT} \exp\left[-\left(\frac{\phi_a - \phi}{kT}\right)\right],$$

where $B(\phi)$ is the distribution function, P_1 is the fractional area, and ϕ_a is the maximum work function. This is illustrated in Fig. XIII-10b. The effects of this distribution on

the output characteristics in region B can be seen by considering the motive diagram, Fig. XIII-10c. As the output voltage is reduced, more of the emitter surface becomes free of the space-charge barrier $\phi_c + V_p + V$, where V_p is the plasma drop. As more of the surface is revealed, more saturation current is obtained from the low work-function patches. The current-voltage relation in region B is given by

$$j_B = j_o\left[1 + \frac{P_1(\phi_a - \phi_c' - V)}{kT}\right], \tag{1}$$

a linear relation between j and V. The fractional area of the exponential patch is given by

$$P_1 = -\frac{kT}{j_o}\frac{dj_B}{dV}. \tag{2}$$

The area is a function of the cesium coverage. From Carabateas,[3] $(T/T_R) = f'(\theta)$ for low coverage. Thus θ is uniquely determined by the temperature ratio and, in fact, decreases in an approximately linear fashion with increasing $\frac{T}{T_R}$. If P_1 is a function of coverage, then its value should also decrease with increasing $\frac{T}{T_R}$.

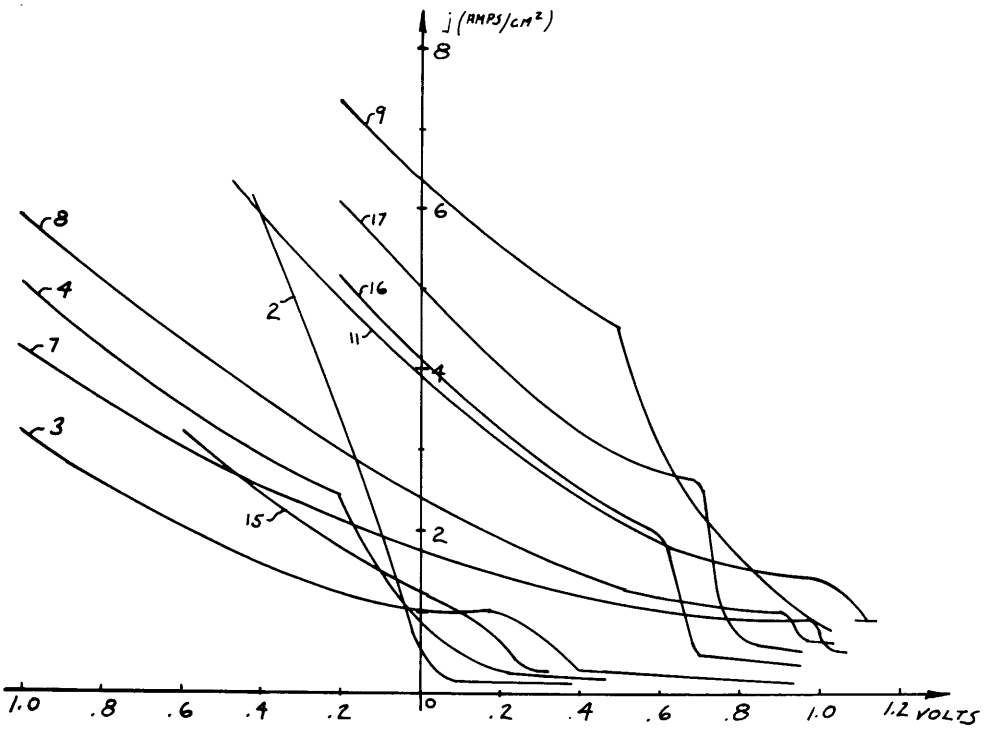

Fig. XIII-11. Experimental I-V curves.

4. Experimental Results

I-V curves obtained at various values of T and T_R appear in Fig. XIII-11. Note that all of the curves display the linear relation in region B given by Eq. 1. Calculated values for P_1 from Eq. 2 appear in Table XIII-2.

The graph of Fig. XIII-12 is a plot of P_1 vs T/T_R, which displays the relation between P_1 and θ.

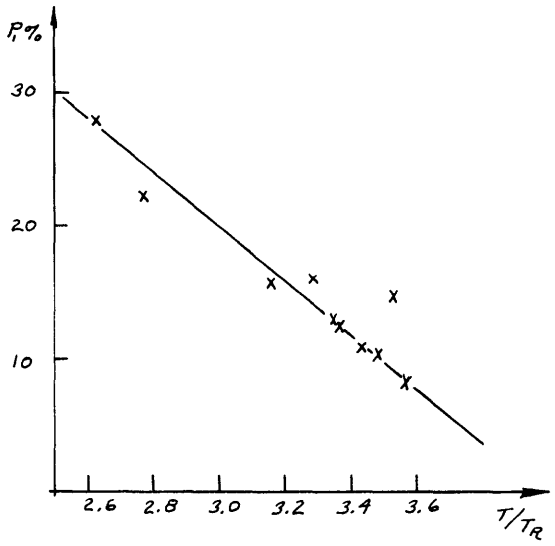

Fig. XIII-12. P_1 versus T/T_R.

Table XIII-2. Diode operating conditions and resulting P_1 from Eq. 2.

Curve	$\frac{T}{(°K)}$	$\frac{T_R}{(°K)}$	$\frac{P_1}{(\%)}$	T/T_R
2	1553	593	28	2.63
3	1693	495	11	3.43
4	1573	478	16.2	3.29
7	1803	510	7.92	3.54
8	1847	530	10.3	3.48
9	1858	555	13	3.35
11	1903	540	14.7	3.53
15	1600	578	22.3	2.77
16	1700	538	15.9	3.16
17	1818	543	12.6	3.35

5. Conclusion

Experimentally obtained current-voltage characteristics of the form shown in Fig. XIII-10 have been interpreted in terms of patches of low work function on the emitter surface. It has been shown that an exponential distribution of work function over a fractional area P_1 of the emitter surface will result in the I-V curves that were obtained, even in the presence of transport effects.

The patches have been shown to be a function of cesium coverage, as shown in Fig. XIII-12. The fractional area of the patches decreases linearly with decreasing cesium coverage. Thus we can conclude that the exponentially distributed patch is caused by thermal excitation of the adsorbed layer. A complete description of this experiment is given in the author's thesis.

J. W. Gadzuk

References

1. I. Psarouthakis, The Design, Construction, and Testing of a Thermionic Energy Converter – Single Crystal Molybdenum Emitter, S. M. Thesis, Department of Mechanical Engineering, M. I. T., May 1962.

2. J. W. Gadzuk, The Effect of Emitter Work Function Patches on the Performance of Cesium Thermionic Converters, S. B. Thesis, Department of Mechanical Engineering, M. I. T., May 1963.

3. E. N. Carabateas, Thermodynamics of surface films, J. Appl. Phys. 33, 2698-2702 (1962).

F. ELECTRON DENSITY IN WET POTASSIUM VAPOR

The energy required to remove one electron from a conducting drop lies somewhere between the ionization potential of a single atom of the metal and the work function associated with an infinite plane surface of the material. This has given rise to speculations regarding the use of condensation drops in alkali-metal vapor magnetohydrodynamic systems.

A number of papers have appeared on the influence of submicroscopic carbon particles on the electron densities in carbon-rich flames. Einbinder,[1] as many others, assumes the following expression for the energy to remove the z^{th} electron from a conducting drop of radius R

$$W = \phi_s + \frac{ze^2}{4\pi\epsilon_o R},$$

where ϕ_s is the flat-surface work function. This expression for z = 1 yields excessive values for W when $R < 100\,\text{Å}$. We have improved the expression by studying the image

forces induced in a conducting sphere by an emitted charge.

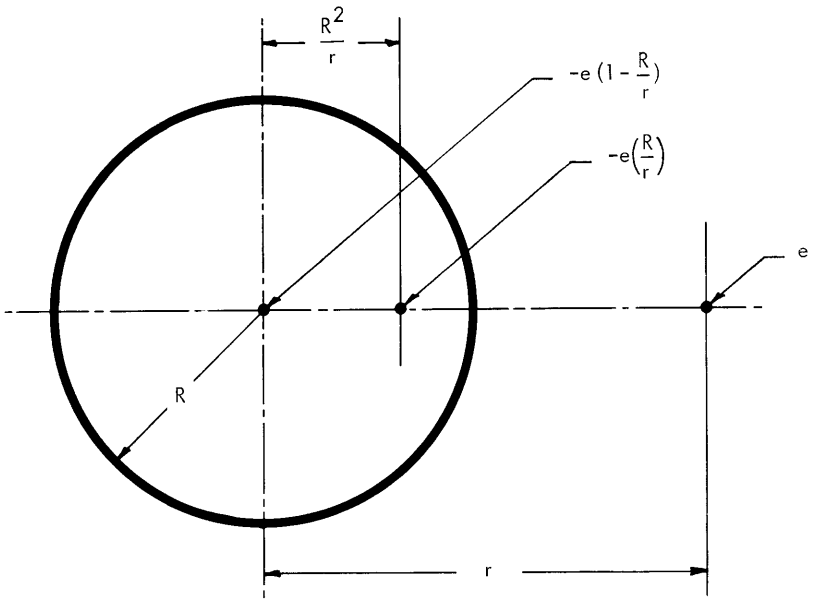

Fig. XIII-13. Induced charges in the spherical conductor.

The ideal force experienced by an electron as a result of induced charges in a drop (Fig. XIII-13) is

$$F(R, r) = \frac{e^2}{4\pi\epsilon_o}\left[\frac{(1-R/r)}{r^2} + \frac{R/r}{(r-R^2/r)^2}\right].$$

Close to the surface of the drop (< 5 Å), the ideal force expression breaks down. We assume that the force behavior at such close distances is independent of drop radius and consequently can remove this unknown behavior by comparing two spheres of different radii.

$$\Delta W = \int_{R+\delta}^{\infty} F(R, r)\, dr - \int_{R'+\delta}^{\infty} F(R', r)\, dr$$

In the limit $R' \to \infty$ and $\delta \to 0$, we find that

$$\Delta W = \phi - \phi_s = \frac{3}{8}\frac{e^2}{4\pi\epsilon_o R},$$

where ϕ is the energy required to remove the first electron from a drop. The work required to remove the z^{th} electron from a drop takes the form

$$W_z = \phi_s + \left[\frac{3}{8} + (z\ 1)\right]\frac{e^2}{4\pi\epsilon_o R}.$$

With this result, equilibrium multiple ionization in a wet potassium vapor has been studied by using a system of Saha equations

$$\frac{N_e N_y^z}{N_y^{z-1}} = 2G\left(\frac{2\pi m_e kT}{h^2}\right)^{3/2} \exp\left(\frac{-W_z}{kT}\right)$$

and the requirements

$$\sum_z N_y^z = N_y$$

$$\sum_y \sum_z Z \cdot N_y^z = N_e.$$

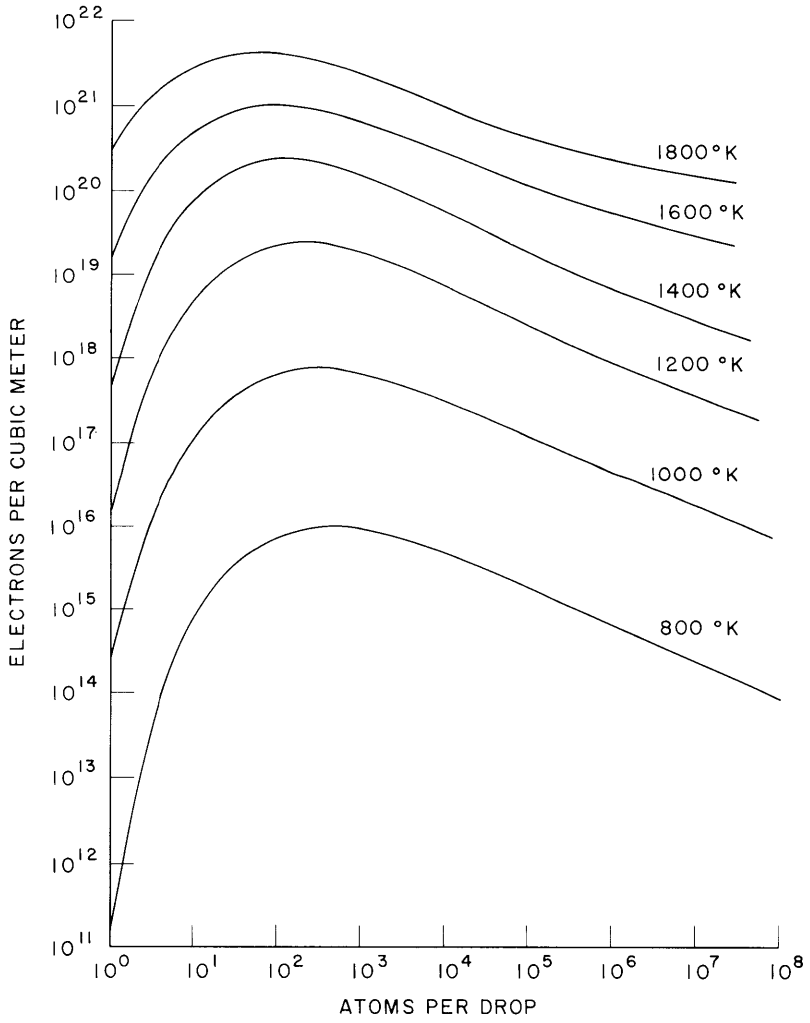

Fig. XIII-14. Electron density in wet potassium vapor.

Here, the lower subscript on particle density N selects particles of a definite size and the superscript further selects those with the same charge. G is the statistical weight equal to 1/2 for potassium atoms, and to unity for drops that differ only in electrostatic charge.

The electron density in a 10 per cent wet potassium vapor was found by using the facilities of the Computation Center, M. I. T. We assumed that all of the drops were of identical size. Figure XIII-14 shows the variation of electron density with vapor temperature and drop size.

It appears that in the plasma studied for this report electron-neutral atom collisions determine the electric conductivity. If this is the case, then the neutral atom-to-electron density ratio governs the conductivity, and the maximum conductivity occurs when the drop size maximizes the electron density in Fig. XIII-14. At 1600°K, the maximum conductivity is 3.5×10^{-1} mho/m as compared with 8.4×10^{-3} mho/m for the dry gas. At lower temperatures the effects of drops are even more pronounced. The implications of these results to magnetohydrodynamic generators continue to be studied.

A. W. Rowe, J. L. Kerrebrock

References

1. H. Einbinder, Generalized equations for the ionization of solid particles, J. Chem. Phys. 26, 948 (1957).